ACCOUNTS
of chemical research

Lithium Insertion in Nanostructured TiO_2(B) Architectures

ANTHONY G. DYLLA, GRAEME HENKELMAN, AND KEITH J. STEVENSON*

Department of Chemistry & Biochemistry, The University of Texas at Austin, Austin, Texas 78712, United States

RECEIVED ON JUNE 12, 2012

CONSPECTUS

Electric vehicles and grid storage devices have potential to become feasible alternatives to current technology, but only if scientists can develop energy storage materials that offer high capacity and high rate capabilities. Chemists have studied anatase, rutile, brookite and TiO_2(B) (bronze) in both bulk and nanostructured forms as potential Li-ion battery anodes. In most cases, the specific capacity and rate of lithiation and delithiation increases as the materials are nanostructured. Scientists have explained these enhancements in terms of higher surface areas, shorter Li^+ diffusion paths and different surface energies for nanostructured materials allowing for more facile lithiation and delithiation. Of the most studied polymorphs, nanostructured TiO_2(B) has the highest capacity with promising high rate capabilities. TiO_2(B) is able to accommodate 1 Li^+ per Ti, giving a capacity of 335 mAh/g for nanotubular and nanoparticulate TiO_2(B). The TiO_2(B) polymorph, discovered in 1980 by Marchand and co-workers, has been the focus of many recent studies regarding high power and high capacity anode materials with potential applications for electric vehicles and grid storage. This is due to the material's stability over multiple cycles, safer lithiation potential relative to graphite, reasonable capacity, high rate capability, nontoxicity, and low cost (Bruce, P. G.; Scrosati, B.; Tarascon, J.-M. Nanomaterials for Rechargeable Lithium Batteries. *Angew. Chem., Int. Ed.* 2008, *47*, 2930−2946). One of the most interesting properties of TiO_2(B) is that both bulk and nanostructured forms lithiate and delithiate through a surface redox or pseudocapacitive charging mechanism, giving rise to stable high rate charge/discharge capabilities in the case of nanostructured TiO_2(B). When other polymorphs of TiO_2 are nanostructured, they still mainly intercalate lithium through a bulk diffusion-controlled mechanism. TiO_2(B) has a unique open crystal structure and low energy Li^+ pathways from surface to subsurface sites, which many chemists believe to contribute to the pseudocapacitive charging.

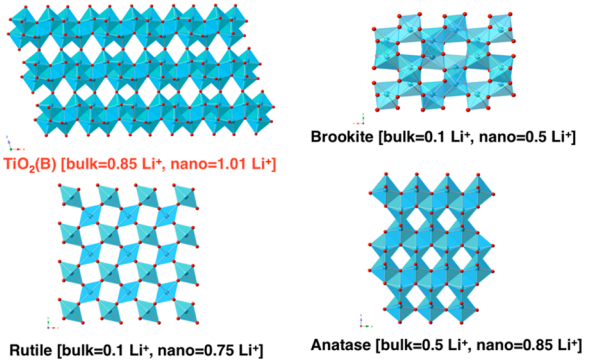

Several disadvantages exist as well. TiO_2(B), and titania in general, suffers from poor electronic and ionic conductivity. Nanostructured TiO_2(B) also exhibits significant irreversible capacity loss (ICL) upon first discharge (lithiation). Nanostructuring TiO_2(B) can help alleviate problems with poor ionic conductivity by shortening lithium diffusion pathways. Unfortunately, this also increases the likelihood of severe first discharge ICL due to reactive Ti−OH and Ti−O surface sites that can cause unwanted electrolyte degradation and irreversible trapping of Li^+. Nanostructuring also results in lowered volumetric energy density, which could be a considerable problem for mobile applications. We will also discuss these problems and proposed solutions.

Scientists have synthesized TiO_2(B) in a variety of nanostructures including nanowires, nanotubes, nanoparticles, mesoporous-ordered nanostructures, and nanosheets. Many of these structures exhibit enhanced Li^+ diffusion kinetics and increased specific capacities compared to bulk material, and thus warrant investigation on how nanostructuring influences lithiation behavior. This Account will focus on these influences from both experimental and theoretical perspectives. We will discuss the surface charging mechanism that gives rise to the increased lithiation and delithiation kinetics for TiO_2(B), along with the influence of dimensional confinement of the nanoarchitectures, and how nanostructuring can change the lithiation mechanism considerably.

1. Introduction

In order for electric vehicles and grid storage devices to become viable alternatives to current technology, further development of energy storage materials that offer high capacity and high rate capabilities is needed.[2,3] Pseudocapacitors can be considered hybrids of traditional batteries

Published on the Web 02/20/2013 www.pubs.acs.org/accounts
10.1021/ar300176y

(high energy density but typically poor power output) and double layer capacitors (high power output during short bursts but low energy density). The pseudocapacitive energy storage mechanism is different from batteries in that surface redox properties dominate the charge-transfer processes rather than normal Faradaic diffusion-controlled insertion processes.[4] Metal oxides such as RuO_2 and IrO_2 act as pseudocapacitors offering exceptional power, fast charging, and long-term stability while also affording some of the advantages of traditional secondary batteries such as reasonable storage capacity.[4,5] Pseudocapacitors with moderate energy density at high charge rates over many cycles could find applications in hybrid-electric or electric vehicles. The pseudocapacitor could be employed when fast power delivery during acceleration is required. Efficient use of renewable energies through load leveling will also require the ability to store and deliver charge rapidly.[3] For these applications, RuO_2 and IrO_2 would be cost prohibitive making, TiO_2 a relatively inexpensive option. By nanostructuring certain electroactive materials, this surface charge-transfer process (pseudocapacitive effect) becomes the dominant storage mechanism and can offer 10−100 times the capacitance of a traditional carbon-based double layer capacitor.[4] As mentioned in the Conspectus, TiO_2(B) is a unique anode material in that both bulk and nanostructured forms lithiate/delithiate through this pseudocapacitive mechanism, making it an attractive material for the applications noted above.

Electrochemical methods have been used to measure Li^+ diffusion kinetics as well as the relative contributions of both capacitive (including double layer capacitance and pseudocapacitance) and diffusion controlled insertion processes to the overall capacity of nanostructured anatase materials.[6,7] More specifically, cyclic voltammetry (CV) can be used to determine the general relationship between current and scan rate by eqs 1 and 2 below:

$$i = \frac{dV}{dt} C_\Phi = \nu C_\Phi \quad (1)$$

$$i = 0.4958nFAc\left(\frac{D\alpha nF\nu}{RT}\right)^{1/2} \quad (2)$$

where C_Φ is surface capacitance, ν is the scan rate, n is the number of electrons, F is the Faraday constant, A is the electrode area, c is the concentration of Li^+, D is the diffusion coefficient, α is the transfer coefficient, R is the gas constant, and T is the temperature. Equation 1 describes capacitive current due to surface confined redox processes (pseudocapacitance) where the current is linear with scan rate.

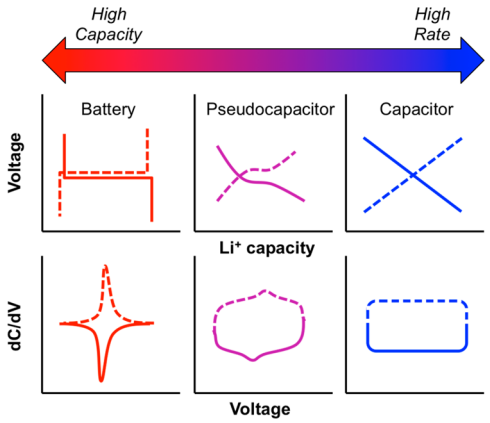

FIGURE 1. Scheme showing idealized voltage and differential capacity (dC/dV) profiles for three basic charge storage mechanisms along with a continuum of their energy storage properties. Pseudocapacitors are attractive because they take advantage of the attractive properties of both batteries (charge storage) and capacitors (high rate delivery or power).

Equation 2 describes current due to normal diffusion controlled Faradaic Li^+ insertion processes where the current is linear with the square root of scan rate. In the case of pseudocapacitance, the extent of charge (Δq) is dependent upon the change in voltage (ΔV), and thus, the total charge passed, d(Δq)/d(ΔV), is the equivalent of capacitance and gives rise to the sloping galvanostatic ($I-V$) profiles often exhibited by those materials.[4] Figure 1 shows a general schematic of the three basic charge storage mechanisms in relation to galvanostatic and differential capacity (dC/dV) plots. Li^+ insertion via pseudocapacitance is similar to a battery in that a redox reaction is required for charge storage but dissimilar in that the process is not diffusion limited.

Wang and co-workers have systematically studied how nanoparticle size affects the relative contributions of pseudocapacitance and bulk diffusion controlled intercalation of Li^+ into nanocrystalline anatase.[9] By combining eqs 1 and 2 above and simplifying to eq 3 below:

$$i(V) = k_1 v + k_2 v^{1/2} \quad (3)$$

They were able to determine relative contributions of pseudocapacitance and diffusion controlled intercalation at a given potential using scan rate studies. Figure 2 shows that as the particle size decreased, the contribution of pseudocapacitance increased as well as slightly increasing the overall storage capacity of the material. The galvanostatic plot shown in Figure 2 also shows the more capacitive-like sloping behavior indicative of this surface charging mechanism.

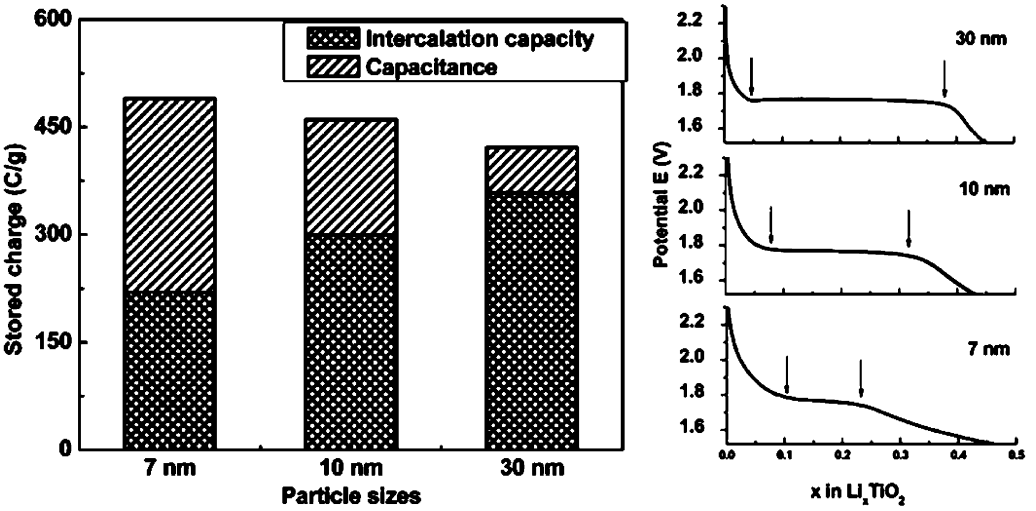

FIGURE 2. Contribution of diffusion controlled capacity and surface capacitance (pseudocapacitance) as a function of anatase nanoparticle size (left) and galvanostatic discharge curves for the three sizes studied (right). Reprinted with permission from ref 9. Copyright 2007 American Chemical Society.

2. The TiO_2(B) Structure

The advantages of using TiO_2 as an anode in rechargeable lithium ion batteries lie in its characteristic safety and stability. Graphite is the most widely used anode material in rechargeable lithium ion batteries due in part to its low lithiation potential (~0.1 V vs Li/Li^+) that allows for a large voltage difference between cathode an anode and reasonably high capacity. The fact that graphite lithiates at a potential near that of the Li/Li^+ couple poses a problem in that the lithium electroplating can cause short circuit and thermal runaway conditions resulting in combustion of organic electrolyte and catastrophic battery failure. Choosing an anode with a higher lithiation potential such as TiO_2 (~1.6 V vs Li/Li^+) greatly reduces the chance of this type of battery failure. Among the common polymorphs, TiO_2(B) has attracted recent attention due mainly to high energy density, but also because of the ability to nanostructure this polymorph into several distinct architectures which provides opportunities to systematically study the charge storage mechanism.

TiO_2(B) was first synthesized in 1980 by Marchand and co-workers from the layered titanate $K_2Ti_4O_9$ which was converted to $H_2Ti_4O_9$ via acid washing and finally dehydrated to the layered TiO_2(B) structure.[10] TiO_2(B) has a monoclinic *C*2/*m* structure comprised of edge- and corner-sharing TiO_6 octahedra with an open channel parallel to the *b*-axis that sits between axial oxygens. Initially TiO_2(B) lithiates as shown in eq 4.

$$x\mathrm{Li} + \mathrm{TiO_2(B)} + xe^- \leftrightarrow \mathrm{Li}_x\mathrm{TiO_2(B)} \quad (4)$$

In subsequent cycles, Li_xTiO_2(B) is reversibly lithiated/delithiated as shown in eq 5.

$$\mathrm{Li}_x\mathrm{TiO_2(B)} \leftrightarrow \mathrm{Li}_{x-y}\mathrm{TiO_2(B)} + y\mathrm{Li}^+ + ye^- \quad (5)$$

The unit cell contains 8 Ti sites and 10 Li^+ sites, giving a theoretical capacity of 1.25 Li^+/Ti (~420 mAh/g), though calculations suggest that because of Li^+–Li^+ repulsions only 8 Li^+ sites can be filled giving a capacity of 1.00 Li^+/Ti (335 mAh/g).[11] Li^+ can bind to three unique sites within the crystal: four A1 and four A2 sites sit near equatorial and axial oxygens in the titania octahera, respectively, and two C sites lie in the open channel along the *b*-axis. Figure 3 shows the crystal structure along with labeled Li^+ site occupations.

Much of the interest in TiO_2(B) as an anode material lies in its unique crystal structure. Compared to other titania polymorphs, TiO_2(B) has the lowest density, and the perovskite-like layered structure along with the open channel parallel to the *b*-axis suggests that fast Li^+ diffusion should be possible. While high rate capabilities have been observed for nanostructured TiO_2(B), the mechanism responsible is still debated.[11] $^7Li^+$ spin-alignment echo nuclear magnetic resonance (SAE-NMR) correlation spectroscopy studies have shown Li^+ self-diffusivity to be quite slow even in nanowire forms of TiO_2(B) suggesting that another mechanism is at play besides facile Li^+ diffusion through the *b*-axis channel in the bulk of the crystal.[12,13] High surface areas and unique surface energetics have been largely invoked to describe the high capacity and rates for nanostructured TiO_2(B).[1]

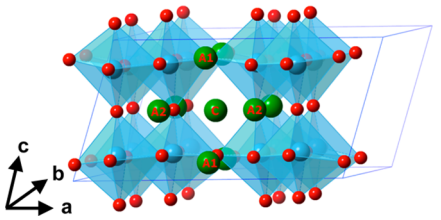

FIGURE 3. Unit cell of TiO_2(B) with idealized Li^+ insertion sites.

3. Lithiation of TiO_2(B)

Bulk TiO_2(B). Bulk TiO_2(B) lithiates to $x = 0.7-0.8$ (Li_xTiO_2(B)) upon first discharge (lithiation) with stable slow rate cycling in the range of $x = 0.3-0.6$.[14−17] The galvanostatic charging/discharging profiles of bulk TiO_2(B) show two distinct plateaus between 1.4 and 1.6 V vs Li/Li^+ upon reduction (intercalation) and similar peaks at slightly higher potentials ($\Delta V \approx 100$ mV) upon oxidation (deintercalation). Zukalova and co-workers were the first to determine the pseudocapacitive Li^+ insertion behavior of TiO_2(B) using scan rate dependent studies on bulk TiO_2(B) showing a linear relationship between scan rate and peak current (see Figure 4).[18]

Nanowires and Nanotubes. Much of the initial research on the lithiation of nanostructured TiO_2(B) comes from Bruce and co-workers on TiO_2(B) nanowires and nanotubes.[16,19,20] Armstrong et al. used a simplified hydrothermal reaction involving anatase powders in KOH solutions to produce the potassium titanate precursor followed by ion exchange in acid to form the hydrogen titanate that was then dehydrated to form TiO_2(B) nanowires and nanotubes.[19,21] They were able to produce either nanotubes or nanowires by controlling the time and temperature of the final dehydration step. Shorter times at lower temperatures produced nanotubes with an external diameter of 10−20 nm and an internal diameter of 5−8 nm with micrometer lengths, while longer times at higher temperatures produced nanowires with 20−40 nm diameters with lengths of several micrometers. Other methods for creating nanowires and nanotubes have been reported including low temperature[22] and microwave[23] methods. In their study of low temperature synthesis methods for producing TiO_2(B) nanowires, Daoud and Pang found that the synthesis of nanotube, nanoribbon, or nanowire structures was highly dependent upon the temperature of the reaction.[22] This suggests that the collapse and dehydration of the layered hydrogen titanate intermediate plays a significant role in the resultant TiO_2(B) nanostructure formed.

The galvanostatic charge/discharge cycles of nanowires and nanotubes typically exhibit redox plateau positions, or redox peaks in differential capacity plots (dC/dV), similar to bulk TiO_2(B). The main difference between the 1-D nanoarchitectures is that the nanotubes have a more sloped profile and increased first cycle ICL relative to the nanowires. Sloping profiles in galvanostatic charge/discharge cycles are often observed for nanostructured Li^+ intercalation materials. This behavior was explained in terms of the curvature of the nanotube walls leading to strain-induced surface free energy changes. As described above, the pseudocapacitive charging mechanism requires that the degree of lithiation be dependent on the potential. In this mechanism, the material's surface acts as a solid solution host to Li^+ insertion and the free energy of the surface changes incrementally as a function of Li^+ concentration. This is in contrast to nanowires that have relatively large widths and less surface strain and act more like bulk materials. The higher degree of ICL for TiO_2(B) nanotubes relative to nanowires was also explained in terms of higher reactivity toward electrolyte decomposition on the strained nanotube surface. The first discharge capacity of TiO_2(B) nanowires and nanotubes at a charge rate of 50 mA/g (0.15 C) was 305 (0.91 Li^+/Ti) and 338 (1.01 Li^+/Ti) mAh/g, respectively. The capacity dropped to 200 and 230 mAh/g, respectively, for the second cycle discharge.

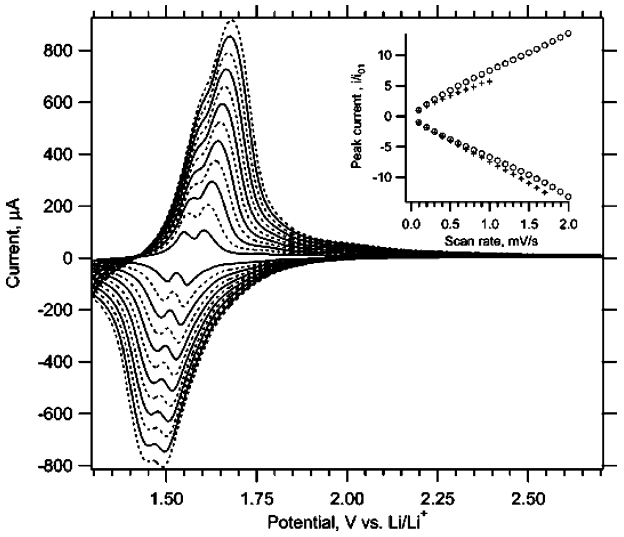

FIGURE 4. Typical cyclic voltammogram of Li^+ insertion and deinsertion into bulk TiO_2(B) along with an inset of the peak current for both oxidation and reduction as a function of scan rate that shows a linear relationship associated with surface charging mechanism. Reprinted with permission from ref 18. Copyright 2005 American Chemical Society.

In terms of specific site filling and lithiation mechanisms, several experimental studies have suggested that facile lithiation occurs radially into the walls of the nanotubes and perpendicular to the flat surface of the nanowires rather than down the long axis of the 1-D structures that is also

parallel to the *b*-axis or C site tunnels.[1,24] Brutti and co-workers used combined FTIR, XPS, and electrochemical studies to investigate the increased ICL observed for nanotube geometries.[25] Earlier work had suggested that either electrolyte decomposition or high-energy surface sites acting as irreversible Li^+ traps during the first lithiation cycle were the cause of the ICL.[24] The latter was ruled out as the main contributor because surface treatments of TiO_2(B) nanotubes with $Li(CH_3CO_2)$ dramatically mitigated the ICL. The lithium acetate reacts with surface Ti−OH to form a Ti−O−Li tube surface that is less reactive toward electrolyte decomposition.

Nanoparticles. The synthesis of TiO_2(B) nanoparticles was first described by Kobayashi and co-workers.[26] They first synthesized a Ti-glycolate complex that was then reacted with H_2SO_4 to form the hydrogen titanate precursor. Finally, the solution of hydrogen titanate was hydrothermally reacted to form nanoparticles of TiO_2(B) in the 3−6 nm size range.

Galvanostatic charging curves of phase-pure TiO_2(B) nanoparticles have only been recently reported by Ren and Bruce.[27] The redox peak positions reported in the d*C*/d*V* plots were similar to those of nanowire and nanotube geometries, implying a similar Li^+ insertion mechanism. The nanoparticle d*C*/d*V* plot does differ from both the nanowire and bulk architectures in that a large capacitive-like region was observed in the 1.4−1.0 V range. This capacitive profile is similar to that observed for nanotubes which may suggest that curvature and/or strain near the surface of these nanomaterials plays an important role in the lithiation mechanism. The first discharge capacity for TiO_2(B) nanoparticles was reported as 322 mAh/g (0.96 Li^+/Ti) at 50 mA/g (0.15 C) charge rate. This discharge capacity is close to the theoretical value, but some ICL is observed upon first charge pointing to redox behavior associated with electrolyte degradation on the first cycle. Upon second discharge at the same rate, the capacity falls to 251 mAh/g (0.75 Li^+/Ti) with good retention upon charge (96%). The nanoparticulate TiO_2(B) outperforms nanotubes, nanowires, and bulk TiO_2(B) in both fast and slow charge rate capacity as can be seen in Figure 5 where several nanoarchitectures of TiO_2(B) along with other titania polymorphs are compared. The authors attributed the enhanced capacity and kinetics of the nanoparticles to increased surface structural distortions making Li^+ transport more facile.

Mesoporous TiO_2(B). As mentioned in the previous sections, high surface area, nanostructured TiO_2(B) with strained surfaces appear to enhance both the capacity and rate

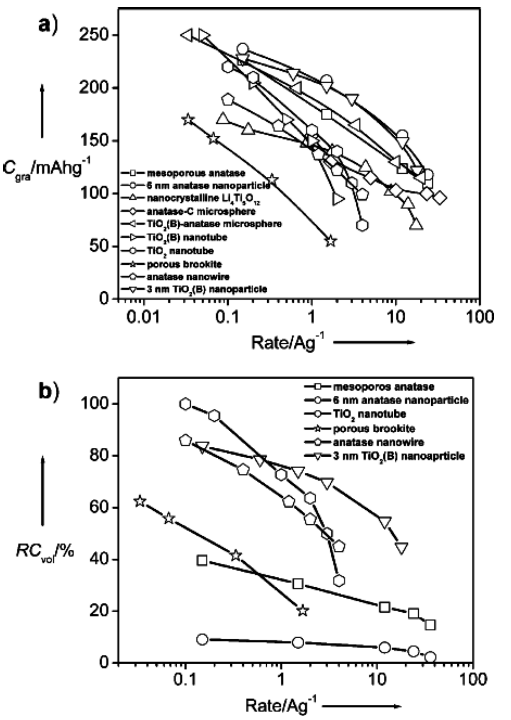

FIGURE 5. Gravimetric capacity (a) and relative volumetric charge retention (b) as a function of charge rate for various TiO_2 nanostructures. Reproduced from ref 27. Copyright 2012 John Wiley & Sons.

capability. Porosity and high surface area has been added to anatase through sol−gel routes involving structure directing diblock copolymers,[28] by templating of preformed anatase nanocrystals,[28] and by reactive ballistic deposition.[29] This increased porosity can enhance both overall storage capacity and high rate capacity due to improved Li-ion coupled electron transfer kinetics, faster diffusion of Li^+ through the interconnected TiO_2 network, and increased electrode/electrolyte contact areas.

Interestingly, when using the sol−gel method for synthesizing mesoporous TiO_2, a second TiO_2 phase is often introduced as a minor component. The hydrolysis conditions required for the formation of Ti−O−Ti oligomeric networks are difficult to control and can result in multiphase materials. Kavan and co-workers noted the impurity during electrochemical experiments showing unique Li^+ insertion at 1.6 V.[30] This phase was first believed to be an amorphous surface anatase species, but was later confirmed to be a TiO_2(B) impurity.[18] In the case of reactive ballistic deposition of titanium in an oxygen environment, Lin and co-workers observed lithium insertion peaks in the cyclic voltammetry similar in position to those found in TiO_2(B) and determined that a mixture of surface pseudocapacitance and diffusion controlled Li^+ insertion was responsible for the charging behavior.[29] These examples point to the complex conditions

that are required to control titania polymorphism at the nanoscale.

Procházka et al. reported on a dip-coating method to produce mesoporous TiO_2(B) on conductive substrates and showed fast lithiation kinetics of the thin films for smart electrochromic window applications.[31] Some anatase contaminants were observed that were likely due to the calcination procedure required to convert the amorphous titania to TiO_2(B). Liu and co-workers recently reported on the lithiation of mesoporous TiO_2(B) microspheres.[32] The advantage of a mesoporous microsphere geometry lies in the ability to increase volumetric energy density due to efficient microsphere packing while maintaining the nanostructure needed for fast surface lithiation kinetics. The CVs showed broad capacitive-like profiles with redox peaks associated with both TiO_2(B) and anatase. The 0.1 C rate capacity was steady at 250 mAh/g after a first cycle capacity of 310 mAh/g, and the material exhibited highly stable charging capacity of 160 mAh/g at 10 C. Recently, Dylla and co-workers reported on the influence of mesoporosity on the rate capability of mesoporously ordered 4−5 nm TiO_2(B) nanoparticles.[33] Using TiO_2(B) nanoparticles as building blocks and a common diblock copolymer (P123) as a structure directing agent, they were able to control the phase purity of the resultant mesoporous thin film structure. They found that the open pore structure enhanced the high rate charging capacity significantly over nontemplated composites of TiO_2(B) nanoparticles and showed through scan rate dependent studies that the mesoporous structures lithiated through a pseudocapacitive mechanism. Similar to the other mesoporous studies, large capacitive-like CVs were observed with the double peak behavior consistent with TiO_2(B) lithium insertion and 170 mAh/g capacity was achieved at a rate of 2.3 C.

Nanosheets. The previous sections on various forms of TiO_2(B) have shown that the kinetics and capacity for lithiation of TiO_2(B) are influenced by both size and architectural control. Ideally then, a flat thin surface of TiO_2(B) should provide superior fast lithiation behavior since the entirety of the material would be considered surface. Xiang and co-workers reported the first synthesis of ultrathin TiO_2(B) nanosheets. Using a simple hydrothermal reaction between ethylene glycol and $TiCl_3$ they were able to produce high purity, atomically thin sheets with nanocrystalline domains throughout the 200−300 nm continuous sheets.[34]

Jang and co-workers were able to produce nanosheet-derived TiO_2(B) that showed promising fast charge rate capacity by condensing a layer-structured titanate ($H_2Ti_4O_9$) into a tunnel-structured titanate ($H_2Ti_8O_{17}$) by heating to 200 °C followed by dehydration at 350 °C.[35] They argued that the increased capacity of the layer-structured derived TiO_2(B) relative to conventional TiO_2(B) was due to the increased surface area. Stable 253 mAh/g capacity was achieved at 100 mA/g (0.3 C). Liu and co-workers used a modified version of the Xiang synthesis to create a porous nanosheet morphology.[36] By adding ammonia to $TiCl_4$ and ethylene glycol in the during solvothermal condensation, they found that a hierarchical pore structure was added to the nanosheets. The cyclic voltammetry studies showed redox peaks similar to other reports for nanostructured TiO_2(B) along with a small amount of anatase byproduct. The first discharge capacity at 34 mA/g (0.1 C) charge rate was 332 mAh/g with significant ICL of 25%. The material showed good high rate capability with highly stable 220 mAh/g capacity at a 10 C charge rate over 200 cycles. They attributed the high rate capability to both the ultrathin geometry and the pore structure that allowed facile access between layers that may otherwise stack on top of one another and therefore be less accessible to electrolyte and would hinder Li^+ diffusion. Most recently, Dylla and co-workers have reported a combined experimental/theoretical study on the lithiation of TiO_2(B) nanoparticles and nanosheets. The experimental dC/dV plots and simulations support significantly different lithiation/delithiation behavior for nanosheets compared to nanoparticles due to the elongated geometry of the nanosheet crystal structure along the *a*-axis.[37]

4. Theoretical Studies

Panduwinata and Gale calculated from first principles the thermodynamics of low concentration Li^+ site occupancy in TiO_2(B).[38] They found the A2 site to be slightly more favorable than the C site due to the increased interactions with neighboring oxygens, five versus two interactions, respectively. Finally, the A1 site was found to be the least favorable due to increased Li^+−Ti repulsions and lattice strain induced by the cation. They also pointed out that there was considerably less lattice expansion within the TiO_2(B) structure compared to anatase or rutile which undergoes significant anisotropic expansions upon Li^+ insertion. Li^+ diffusion in the dilute limit was also explored, and diffusion from C sites to A2 sites was found to be lowest in energy followed by A2 to C and A1 to C. These three lowest energy diffusion barriers all occur in either the *a*- or *c*-axis direction which are known to be parallel to radial diffusion in TiO_2(B) nanotubes and nanowires. These calculations correlate well with the experimental results showing increased rate capability for the nanotube geometry that allows for radial diffusion through the *a*- and *c*-axes. Contrary to these results, Arrouvel and

co-workers used DFT to calculate an off-centered C site as being most stable at low Li^+ concentrations followed by A2 and A1 site occupation.[39] They also calculated diffusion along the *b*-axis to be most favorable although they only considered C-to-C site diffusion, which again is in contradiction to the calculations of Panduwinata and Gale.

In a combined DFT and experimental study, Islam and co-workers found C-site binding to be preferential followed by A2 and A1. However, speculation of anatase impurities mixed with the TiO_2(B) used in this study may have led to an incorrect interpretation of the data.[40] They also argued that the curved surfaces of these nanostructures would be a hindrance to diffusion into the interior of the structure due to compression in the *a*−*b* plane as Li^+ diffused deeper into radius of the 1-D structures. Using DFT calculations, Koudriachova showed A1 site absorption on (001) surfaces to be favorable and connected to subsurface A2 sites via low energy diffusion pathways in the *c*-axis direction until all of the A2 sites had been filled, leading to 0.5 Li^+/Ti.[41] This low energy diffusion pathway was thought to contribute to the pseudocapacitive behavior of TiO_2(B) in nanowires and nanotubes which have a stretched surface allowing for minimization of Li^+−Ti interactions from the A1 surface sites to the A2 subsurface sites. Recently, Dalton and co-workers used DFT in combination with Monte Carlo simulations to predict Li^+ site occupancies as well as voltage curves and phase diagrams.[42] Their calculations showed A1 to be the most stable site at low Li^+ concentrations followed by A2. The C site was shifted in the *b*-axis direction but was still highly unfavorable compared to A1 and A2 site occupancy. Upon filling to $x = 0.25$, A1 sites are filled on different planes in the *c*-axis direction and all of A1 sites are filled at $x = 0.5$. At $x = 0.75$, an inversion occurs that causes A2 and C sites to be filled in the (001) plane. Finally, at $x = 1.0$, all of the A2 and C sites are filled.

In the previously mentioned theoretical studies, the energy penalty (+U) was not included in the calculations. Morgan and Watson recently showed that DFT alone is inadequate to describe Li^+ binding in anatase because of the delocalization of 3d electrons over all Ti centers.[43] Only by adding the energy penalty that forces 3d electrons to localize at Ti centers does the theory predict the expected Li^+ site occupation behavior. Most, recently Dylla and co-workers showed in a combined experimental and DFT+U study that site filling preferences change as a function of nanoarchitecture.[37] For 3-D structures such as bulk and nanoparticles, the preference for filling follows A2 > C > A1 at the dilute limit with A2 and C being close in energy. Upon

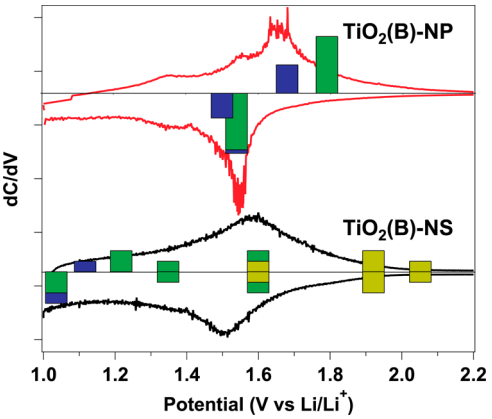

FIGURE 6. Differential capacity plots of TiO_2(B) nanoparticles (NP-top) and nanosheets (NS-bottom) at 50 mA/g charge rate along with an overlay of DFT+U calculated lithiation/delithiation potentials and relative Li^+ concentrations (height) for the lithiation/delithiation process. The histogram colors correlate to the intercalation sites being filled: blue = A1, green = A2, and yellow = C. Reprinted with permission from ref 37. Copyright 2012 American Chemical Society.

lithiation, all of the A2 sites are filled, followed by alternating A1 sites until $x = 0.75$. Similar to the work by Dalton and co-workers,[42] the symmetric C site was found to be unstable due to Li^+−Li^+ repulsions from neighboring A2 sites and a new site was found shifted in the *b*-axis direction though was found to be filled at extremely low voltages out of the range typically studied experimentally. In contrast, TiO_2 nanosheets were calculated to favorably lithiate at the C sites at low concentrations followed by A2 sites and A1 sites. The difference in calculated site filling between the 2-D and 3-D nanostructures was attributed to the relaxed calculated TiO_2(B) nanosheet architecture that allows for decreased Li^+−Li^+ repulsions at A2 and C sites allowing for favorable C site binding and a shifting in the A2 site away from the ideal axial position. Figure 6 shows a comparison of dC/dV plots along with histogram overlays of the DFT+U derived Li^+ site occupancy voltages and relative concentrations.

5. Challenges and Future Prospects

While the high surface energy architectures such as nanotubes and nanoparticles provide facile lithiation kinetics, they are often coupled with ICL associated with electrolyte degradation occurring on those same high energy sites. The nanosheet geometry may be the best option to take advantage of both the high capacity and rates offered by these nanoarchitectures while avoiding significant ICL as the surface strain effect should be lessened for the flexible sheets. Furthermore, any nanoarchitecture used in a battery where volumetric power or energy density is of concern; that is, mobile and vehicle applications will require a hierarchical

assembly of nanomaterials into larger micrometer-sized structures in order to increase tap and volumetric energy density. Previously mentioned work by Liu and co-workers on 200−300 nm sized clusters with petal-like sheets of TiO_2(B) radiating out from the core presents a step in the right direction in this regard.[36] Surface protectants may be another way of mitigating ICL in nanoarchitectured TiO_2(B) as shown above by Brutti and co-workers in the case of TiO_2(B) nanowires.[25]

Throughout this Account, we have shown that TiO_2(B) has unique and complex lithiation/delithiation behavior. A full understanding of why nanostructuring is so influential of the high rate capability and high capacity is still an open question. It appears that more surface analytical studies and calculations of surface Li^+ binding on various TiO_2(B) surfaces are warranted as the majority of the charging behavior seems to be controlled by surface interactions rather than the bulk.

BIOGRAPHICAL INFORMATION

Anthony Dylla received his Ph.D. from the University of Maryland in 2009 on the synthesis, characterization, and catalytic properties of bimetallic nanoparticles. He is currently a postdoctoral fellow at the University of Texas at Austin. His research interests are in nanostructured metal oxides and the use of in situ vibrational spectroscopy to study materials relevant to energy storage.

Graeme Henkelman received his Ph.D. from the University of Washington in 2001. He was a postdoctorate fellow at Los Alamos National Laboratory from 2002 to 2004 and is now associate professor at the University of Texas at Austin. His research interests include DFT and Monte Carlo studies of catalytic and energy storage related materials.

Keith Stevenson received his Ph.D. from the University of Utah in 1997. He was a postdoctorate fellow at Northwestern University from 1997 to 2000 and is now full professor at the University of Texas at Austin. His research interests include nanostructured materials for energy storage, electroanalytical and surface chemistry, electrochemical sensors, and development of high-resolution analytical tools and methods.

FOOTNOTES

*To whom correspondence should be addressed. E-mail: stevenson@cm.utexas.edu.
The authors declare no competing financial interest.

REFERENCES

1 Bruce, P. G.; Scrosati, B.; Tarascon, J.-M. Nanomaterials for Rechargeable Lithium Batteries. *Angew. Chem., Int. Ed.* **2008**, *47*, 2930–2946.

2 Wagner, F. T.; Lakshmanan, B.; Mathias, M. F. Electrochemistry and the Future of the Automobile. *J. Phys. Chem. Lett.* **2010**, *1*, 2204–2219.

3 Yang, Z.; Zhang, J.; Kintner-Meyer, M. C. W.; Lu, X.; Choi, D.; Lemmon, J. P.; Liu, J. Electrochemical Energy Storage for Green Grid. *Chem. Rev.* **2011**, 1–37.

4 Conway, B. E. *Electrochemical Supercapacitors*; Kluwer Academic/Plenum Publishers: New York, 1999; pp 221−241.

5 Conway, B. E. Transition from supercapacitor to battery behavior in electrochemical energy-storage. *J. Electrochem. Soc.* **1991**, *138*, 1539–1548.

6 Lindstrom, H.; Sodergren, S.; Solbrand, A.; Rensmo, H.; Hjelm, J.; Hagfeldt, A.; Lindquist, S. Li+ ion insertion in TiO_2 (anatase). 1. Chronoamperometry on CVD films and nanoporous films. *J. Phys. Chem. B* **1997**, *101*, 7710–7716.

7 Lindstrom, H.; Sodergren, S.; Solbrand, A.; Rensmo, H.; Hjelm, J.; Hagfeldt, A.; Lindquist, S. Li+ ion insertion in TiO_2 (anatase). 2. Voltammetry on nanoporous films. *J. Phys. Chem. B* **1997**, *101*, 7717–7722.

8 Bard, A. J.; Faulkner, L. R. *Electrochemical Methods: Fundamentals and Applications*; John Wiley & Sons: New York, 2001.

9 Wang, J.; Polleux, J.; Lim, J.; Dunn, B. Pseudocapacitive Contributions to Electrochemical Energy Storage in TiO_2 (Anatase) Nanoparticles. *J. Phys. Chem. C* **2007**, *111*, 14925–14931.

10 Marchand, R.; Brohan, L.; Tournoux, M. TiO_2(B) A new form of titanium-dioxide and the potassium octatitanate $K_2Ti_8O_{17}$. *Mater. Res. Bull.* **1980**, *15*, 1129–1133.

11 Okumura, T.; Fukutsuka, T.; Yanagihara, A.; Orikasa, Y.; Arai, H.; Ogumi, Z.; Uchimoto, Y. Electronic and local structural changes with lithium-ion insertion in TiO_2-B: X-ray absorption spectroscopy study. *J. Mater. Chem.* **2011**, *21*, 15369.

12 Wilkening, M.; Heine, J.; Lyness, C.; Armstrong, A.; Bruce, P. Li diffusion properties of mixed conducting TiO_2-B nanowires. *Phys. Rev. B* **2009**, *80*, 064302.

13 Wilkening, M.; Lyness, C.; Armstrong, A. R.; Bruce, P. G. Diffusion in Confined Dimensions: Li^+ Transport in Mixed Conducting TiO_2−B Nanowires. *J. Phys. Chem. C* **2009**, *113*, 4741–4744.

14 Zachauchristiansen, B.; West, K.; Jacobsen, T.; Atlung, S. Lithium insertion in different TiO_2 modifications. *Solid State Ionics* **1988**, *28*, 1176–1182.

15 Zachauchristiansen, B.; West, K.; Jacobsen, T.; Skaarup, S. Lithium insertion in isomorphous MO_2(B) structures. *Solid State Ionics* **1992**, *53*, 364–369.

16 Armstrong, A.; Armstrong, G.; Canales, J.; Garcia, R.; Bruce, P. Lithium-ion intercalation into TiO_2-B nanowires. *Adv. Mater.* **2005**, *17*, 862–865.

17 Inaba, M.; Oba, Y.; Niina, F.; Murota, Y.; Ogino, Y.; Tasaka, A.; Hirota, K. TiO_2(B) as a promising high potential negative electrode for large-size lithium-ion batteries. *J. Power Sources* **2009**, *189*, 580–584.

18 Zukalova, M.; Kalbac, M.; Kavan, L.; Exnar, I.; Graetzel, M. Pseudocapacitive lithium storage in TiO_2(B). *Chem. Mater.* **2005**, *17*, 1248–1255.

19 Armstrong, A. R.; Armstrong, G.; Canales, J.; Bruce, P. G. TiO_2-B Nanowires. *Angew. Chem., Int. Ed.* **2004**, *43*, 2286–2288.

20 Armstrong, A.; Armstrong, G.; Canales, J.; Bruce, P. TiO_2-B nanowires as negative electrodes for rechargeable lithium batteries. *J. Power Sources* **2005**, *146*, 501–506.

21 Armstrong, G.; Armstrong, A. R.; Canales, J.; Bruce, P. G. Nanotubes with the TiO_2-B structure. *Chem. Commun.* **2005**, 2454.

22 Daoud, W. A.; Pang, G. K. H. Direct Synthesis of Nanowires with Anatase and TiO_2-B Structures at near Ambient Conditions. *J. Phys. Chem. B* **2010**, 1–5.

23 Qiao, Y.; Hu, X.; Huang, Y. Microwave-induced solid-state synthesis of TiO_2(B) nanobelts with enhanced lithium-storage properties. *J. Nanopart. Res.* **2012**, *14*, 1–7.

24 Armstrong, G.; Armstrong, A. R.; Canales, J.; Bruce, P. G. TiO_2(B) Nanotubes as Negative Electrodes for Rechargeable Lithium Batteries. *Electrochem. Solid St.* **2006**, *9*, A139–A143.

25 Brutti, S.; Gentili, V.; Menard, H.; Scrosati, B.; Bruce, P. G. TiO_2-(B) Nanotubes as Anodes for Lithium Batteries: Origin and Mitigation of Irreversible Capacity. *Adv. Energy Mater.* **2012**, *2*, 322–327.

26 Kobayashi, M.; Petrykin, V. V.; Kakihana, M. One-step synthesis of TiO_2(B) nanoparticles from a 'Water-Soluble titanium complex. *Chem. Mater.* **2007**, *19*, 5373–5376.

27 Ren, Y.; Bruce, P. G. Nanoparticulate TiO_2(B): An Anode for Lithium-Ion Batteries. *Angew. Chem., Int. Ed.* **2012**, *51*, 2164–2167.

28 Brezesinski, T.; Wang, J.; Polleux, J.; Dunn, B.; Tolbert, S. H. Templated Nanocrystal-Based Porous TiO_2 Films for Next-Generation Electrochemical Capacitors. *J. Am. Chem. Soc.* **2009**, *131*, 1802–1809.

29 Lin, Y. M.; Abel, P. R.; Flaherty, D. W.; Wu, J.; Stevenson, K. J.; Heller, A.; Mullins, C. B. Morphology Dependence of the Lithium Storage Capability and Rate Performance of Amorphous TiO_2 Electrodes. *J. Phys. Chem. C* **2011**, *115*, 2585–2591.

30 Kavan, L.; Rathouský, J.; Grätzel, M.; Shklover, V.; Zukal, A. Surfactant-Templated TiO_2 (Anatase): Characteristic Features of Lithium Insertion Electrochemistry in Organized Nanostructures. *J. Phys. Chem. B* **2000**, *104*, 12012–12020.

31 Procházka, J.; Kavan, L.; Zukalová, M.; Frank, O.; Kalbáč, M.; Zukal, A.; Klementová, M.; Carbone, D.; Graetzel, M. Novel Synthesis of the TiO_2(B) Multilayer Templated Films. *Chem. Mater.* **2009**, *21*, 1457–1464.

32 Liu, H.; Bi, Z.; Sun, X.-G.; Unocic, R. R.; Paranthaman, M. P.; Dai, S.; Brown, G. M. Mesoporous TiO_2-B Microspheres with Superior Rate Performance for Lithium Ion Batteries. *Adv. Mater.* **2011**, *23*, 3450–3454.

33 Dylla, A. G.; Lee, J. A.; Stevenson, K. J. Influence of Mesoporosity on Lithium-Ion Storage Capacity and Rate Performance of Nanostructured TiO_2(B). *Langmuir* **2012**, *28*, 2897–2903.

34 Xiang, G.; Li, T.; Zhuang, J.; Wang, X. Large-scale synthesis of metastable TiO_2(B) nanosheets with atomic thickness and their photocatalytic properties. *Chem. Commun.* **2010**, *46*, 6801–6803.

35 Jang, H.; Suzuki, S.; Miyayama, M. Synthesis of open tunnel-structured TiO_2(B) by nanosheets processes and its electrode properties for Li-ion secondary batteries. *J. Power Sources* **2012**, *203*, 97–102.

36 Liu, S.; Jia, H.; Han, L.; Wang, J.; Gao, P.; Xu, D.; Yang, J.; Che, S. Nanosheet-Constructed Porous TiO_2-B for Advanced Lithium Ion Batteries. *Adv. Mater.* **2012**, *24*, 3201–3204.

37 Dylla, A. G.; Xiao, P.; Henkelman, G.; Stevenson, K. J. Morphological Dependence of Lithium Insertion in Nanocrystalline TiO_2(B) Nanoparticles and Nanosheets. *J. Phys. Chem. Lett.* **2012**, *3*, 2015–2019.

38 Panduwinata, D.; Gale, J. D. A first principles investigation of lithium intercalation in TiO_2-B. *J. Mater. Chem.* **2009**, *19*, 3931–3940.

39 Arrouvel, C.; Parker, S. C.; Islam, M. S. Lithium Insertion and Transport in the TiO_2-B Anode Material: A Computational Study. *Chem. Mater.* **2009**, *21*, 4778–4783.

40 Armstrong, A. R.; Arrouvel, C.; Gentili, V.; Parker, S. C.; Islam, M. S.; Bruce, P. G. Lithium Coordination Sites in Li_xTiO_2(B): A Structural and Computational Study. *Chem. Mater.* **2010**, *22*, 6426–6432.

41 Koudriachova, M. V. Role of the surface in Li insertion into nanowires of TiO_2-B. *Surf. Interface Anal.* **2010**, *42*, 1330–1332.

42 Dalton, A. S.; Belak, A. A.; Van der Ven, A. Thermodynamics of Lithium in TiO_2(B) from First Principles. *Chem. Mater.* **2012**, *24*, 1569–1574.

43 Morgan, B. J.; Watson, G. W. GGA+ U description of lithium intercalation into anatase TiO_2. *Phys. Rev. B* **2010**, *82*, 144119.